A Fatigue Life Model for Predicting Crack Nucleation at Inclusions in Ni-Based Superalloys

KWAI S. CHAN

Engineering alloys such as Ni-based alloys, Al-alloys, and steels often contain non-metallic inclusions in their microstructures. These inclusions, which include oxide particles, carbides, and intermetallic particles, are introduced during component manufacturing processes such as casting, powder-metallurgy, or additive manufacturing methods. The presence of inclusions in the microstructure can promote fatigue crack nucleation by competing against slipband nucleation and reduce fatigue life performance of an engineering component. While it has been reported in many occasions, the competition between fatigue crack nucleation at inclusions and slipbands is still not well understood. In this article, the conditions for the concurrent occurrence of fatigue crack nucleation at inclusions and slipbands are analyzed theoretically. The analysis indicates that there exists a critical inclusion size (diameter) below which there is no fatigue life debit due to crack initiation at inclusions and above which a transition from slip-induced to inclusion-induced crack nucleation occurs. The low-cycle fatigue life model is applied to Ni-based superalloys and the model predictions are compared against experimental data from the literature to assess the dependence of the critical inclusion size on the slip morphology, grain size of the matrix, and the shear modulus of the inclusion.

https://doi.org/10.1007/s11661-019-05592-4

I. INTRODUCTION

STRUCTURAL alloys such as steels,[1] Al-alloys,[2–6] and Ni-based superalloys[7–21] often contain non-metallic inclusions in the microstructure. These inclusions can serve as fatigue crack nucleation sites during cyclic loading conditions, thereby promoting the onset of fatigue failure and reducing the cycles-to-failure or fatigue life. Powder-metallurgy (PM)[7–9,14–22] and additively manufactured (AM) superalloy[23,24] components are particularly disposed to exhibiting inclusions in the microstructure since they are processed using powder particles that can be mixed with small amounts of non-metallic inclusions. As a result, there has been considerable interest in characterizing and studying the influence of inclusions on the fatigue life of forged,[10–13] PM[14–21] and AM[21,22] superalloy materials. For examples, carbide-induced fatigue fracture was studied for forged IN-718 by Späth *et al.*,[11] Ono *et al.*,[12] and Bhowal *et al.*[13] Späth *et al.*[11] showed that the fatigue life of IN 718 increased with increasing ASTM grain size number (*i.e.*, decreasing grain size). In addition, fatigue lives were lowered when crack nucleation switched from slipbands to small carbides.[11] Inclusion-initiated fatigue fracture was investigated for PM Astroloy,[20,21] Rene 95,[14–16] Rene 88 DT,[17,18] and ME3,[22] as well as for AM 718Plus.[23,24] Inclusions that have been identified as crack nucleation sites in Ni-based superalloys include Al_2O_3,[16,20,21] MgO,[21] SiO_2,[21] carbides,[10–13] and nitrides.[10] These non-metallic inclusions (NMI) can manifest as hard particles or granular agglomerates.[14,15,20] Most of the inclusion-induced nucleation occur in interior grains but some may lie near the surfaces, while slipband-induced crack nucleation also can occur in interior and surface grains.[7–10,17–22,25,26] The transition of interior nucleation at inclusions to surface nucleation at matrix grains was also reported in a number of investigations.[7–10,17–22,25,26] Furthermore, the concurrent occurrence of slipband facets, which are evidence of slipband-induced nucleation, and inclusion-induced facets, which are evidence of inclusion-induced nucleation, in individual fatigue specimens has been reported, but the reason for its occurrence is not well understood.

Early studies of correlations of oxide inclusion and fatigue fracture were reviewed by Lankford,[1] who reported an empirical relation between a fatigue strength reduction factor and inclusion size to a power of − 1/3. Micromechanics-based fatigue life models for slipband nucleation and inclusion nucleation were proposed by Tanaka and Mura[27,28] and extended by Chan.[29,30] Statistical models of crack nucleation at inclusions were

KWAI S. CHAN is with the Southwest Research Institute, San Antonio, TX 78238 and also now with the MESI Technologies LLC, San Antonio, TX 78250. Contact e-mail: kchansatx@icloud.com
Manuscript submitted August 9, 2019.
Article published online December 17, 2019

proposed by Morris and James[6] for Al-alloys on the basis of a dislocation pile-up model[5] and by Bussac and Lautridou[31] for PM Ni-based superalloys. Alexandre *et al.*[10] modeled the optimum grain size for the transition of slipband-induced nucleation to inclusion-induced nucleation in forged IN-718 using a proposed relation between cycle-to-crack nucleation (N_i) and $1/D$, where D is the matrix grain size. Similarly, a semi-empirical relation between N_i and $1/D$ was proposed Morris and James[6] for treating fatigue fracture of intermetallic particles by impinging slip in Al-alloys. In contrast, Murakami *et al.*[32,33] proposed a fatigue limit model that treats the area of the cracked inclusion as an internal small-crack, whose growth kinetics is governed by a fatigue crack growth threshold, ΔK_{th}. More recently, Jiang *et al.*[33,34] utilized electron back-scattered diffraction and high-resolution digital image correlation to measure the plastic strains and geometric necessary dislocation (GND) accumulation at and around inclusions[33,34] and modeling the fatigue damage processes in the vicinity of the inclusions using finite-element analysis.[35] Zhang *et al.*[36] combined these experimental techniques with a crystal plasticity finite-element model to analyze crack nucleation at the interface of matrix/inclusion in a superalloy. None of the existing models, however, provide an explanation for the occurrence of concurrent slipband-induced and inclusion-induced crack nucleation observed in Ni-based superalloys.

The important role of inclusions in fatigue crack nucleation in Ni-based superalloys is well recognized and the dependence of fatigue life of Ni-based superalloys on the cleanliness and inclusion content is well established.[20,37,38] The location, size, type, number density, and the occurrence rate of inclusions can exert significant influence on the fatigue crack nucleation and growth lives of Ni-based superalloys.[6–10,20,25,37,38] The interactions of the location, size, type, and number density of anomalies such as pores and non-metallic inclusions on the fatigue life of Ni-based superalloys have been investigated by Enright and McClung[39] using a probabilistic damage tolerance approach. The earlier study, however, did not consider the effects of grain size on the fatigue crack nucleation process. Recent works on IN 718DA[40–42] and GH4169,[43,44] which is similar to IN 718, have demonstrated that a fine-grained microstructure can result in large variability of fatigue life of IN 718DA and GH4169 due to crack nucleation at small carbides. Thus, there exists a need to develop a better understanding of the role of grain size in fatigue crack nucleation at non-metallic inclusions.

In this article, a theoretical analysis is performed to assess the microstructural condition(s) that are conducive to the concurrent occurrence of slipband-induced and inclusion-induced crack nucleation in Ni-based superalloys and the possible implications on fatigue life. The approach is to start with two existing microstructure-based fatigue life models,[29,30] one for slipband nucleation and one for inclusion-based nucleation, and then determine under what microstructural conditions, as represented by the values of relevant material parameters, that would provide identical fatigue life for the concurrent occurrence of slipband-induced and inclusion-induced nucleation. The analysis indicates the existence of a critical inclusion size below which there is no fatigue life debit due to the presence of inclusions in the microstructure and the corresponding fatigue life is controlled by slipband-induced crack nucleation. At or above the critical inclusion size, the fatigue life for inclusion-induced nucleation decreases with increasing inclusion size according to a power-law. These model results are compared against experimental data in the literature to evaluate the validity of the proposed model for Ni-based superalloys manufactured by wrought, PM, or AM techniques. The experimental evidence provide strong support for the power-law scaling law and the existence of a critical inclusion size in Ni-based superalloys.

II. MODEL FORMULATION

The fatigue crack nucleation mechanisms considered in this article are shown schematically in Figures 1(a) and (b), which show fatigue crack nucleation at a

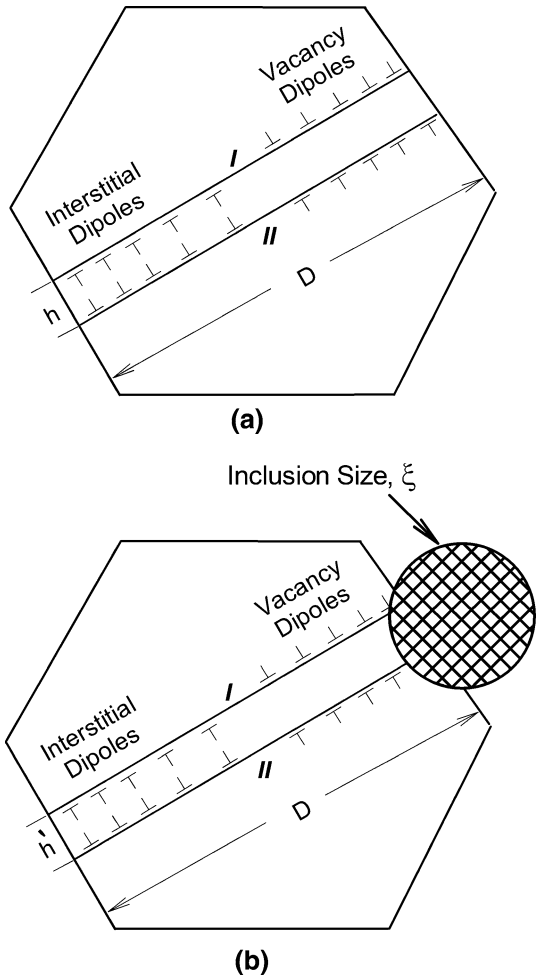

Fig. 1—Schematics of slip-induced fatigue crack nucleation: (*a*) crack nucleation along slipband, and (*b*) crack nucleation at an inclusion of size (diameter) ξ.

slipband and at an inclusion impinged by a slipband, respectively. It is noted that the slipband width, h, involved in slipband crack nucleation in Figure 1(a) is different from the slipband width, h', involved in inclusion-induced crack nucleation in Figure 1(b). In particular, h and h' are not drawn to scale and are expected to have different values. In previous investigations,[29,30] h and h' are assumed to be identical; this restriction is unnecessary and is now removed in this investigation. As reported previously, the fatigue model for crack initiation at slipband has the form given by[29,30]

$$N_i^{\mathrm{S}} = \left[\frac{\zeta_{\mathrm{S}}}{\left(\frac{2\sigma_{\mathrm{a}}}{F_{\mathrm{m}}} - 2Mk\right)}\right]^{1/\alpha} \qquad [1]$$

$$\text{with } \zeta_{\mathrm{S}} = \left[\frac{8M^2\mu^2}{\lambda'\pi(1-\nu)}\right]^{1/2}\left(\frac{h}{D}\right)\left(\frac{c}{D}\right)^{1/2} \qquad [2]$$

$$\text{and } F_{\mathrm{m}} = 1 - \left(\frac{\sigma_{\mathrm{m}}}{\sigma_{\mathrm{UTS}}}\right)^{\beta}, \qquad [3]$$

where N_i^{S} is the cycle-to-crack nucleation at slipbands, σ_{a} is the stress amplitude, M is the Taylor factor, and k is the critical resolved shear stress (friction stress) for slip, α is the fatigue life exponent, ζ_{s} represents the resistance of the microstructure against fatigue crack initiation at slipbands, and F_{m} accounts for the decrease of fatigue resistance with increasing mean stress σ_{m} (one-half of the sum of the maximum and minimum stresses) of a fatigue cycle. In Eq. [2], μ is shear modulus, ν is Poisson's ratio, h is slipband width, D is grain size, c is the dislocation pile-up length or crack length at crack initiation, and λ' is a universal constant with a value of 0.005. In Eq. [3], σ_{UTS} is the ultimate tensile strength, and β is an empirical constant. The Goodman relation is obtained when $\beta = 1$. Positive deviation from the Goodman relation occurs when $\beta > 1$ and negative deviation is obtained when $\beta < 1$. The microstructural input to the *slipband crack initiation* model is the grain size (D) and the slipband width (h). The dislocation pile-up length, c, is on the order of one to a few grain diameters. Fatigue crack nucleation at slipbands does not explicitly depend on the γ' size in Ni-based superalloys but shearing of the ordered precipitates (such as γ' or γ'') would promote slipband cracking. It should also be emphasized that the inclusion level in powder-metallurgy (PM) Ni-based superalloys is controlled by the cleanliness of the fine powder.[20,37,38] Currently, fine powders (<– 270 mesh) with inclusion contamination levels less than 1 ppm by weight can be achieved.[38] Thus, the occurrence rate of slipband impinging at large non-metallic inclusions would depend strongly on the inclusion level in the Ni-based superalloys.

For fatigue crack nucleation at inclusions, the fatigue model for crack initiation at inclusions proposed by Chan[29,30] has the form given by

$$N_i^{\mathrm{I}} = \left[\frac{\zeta_I}{\left(\frac{2\sigma_{\mathrm{a}}}{F_{\mathrm{m}}} - 2Mk\right)}\right]^{1/\alpha} \qquad [4]$$

$$\text{with } \zeta_{\mathrm{I}} = \left[\frac{8(\mu+\mu')}{\lambda'\mu'}\right]^{1/2}\left(\frac{M\mu h'^2}{D\left(\frac{D}{2}+h'\right)}\right)\left(\frac{c}{\xi}\right)^{1/2}, \qquad [5]$$

where N_i^{I} is the cycle-to-crack initiation at inclusion, ζ_{I} represents the resistance of the microstructure against fatigue crack initiation at inclusions, and F_{m}, given by Eq. [3], accounts for the decrease of fatigue resistance with increasing mean stress σ_{m} (one-half of the sum of the maximum and minimum stresses) of a fatigue cycle. In Eq. [5], μ' is the shear modulus of the inclusion, h' is the width of the slipband impinging on the inclusion, D is the matrix grain size, c is the dislocation pile-up length or crack length at crack initiation, and ξ is the inclusion size. The microstructural input to the *crack initiation* model for inclusion is the grain size (D), the slipband width (h'), and the inclusion size (ξ).

A comparison of Eqs. [1] and [4] reveals that crack nucleation at inclusion is affected by properties of both the matrix and the inclusion. Equation [4] can be rearranged and expressed in terms of the matrix and inclusion properties. Using this approach, the cycles-to-crack nucleation at an inclusion can be expressed in terms of matrix properties as given by

$$N_i^{\mathrm{I}} = N_i^{\mathrm{S}}\left[\frac{\xi}{\xi_{\mathrm{o}}}\right]^{-1/(2\alpha)}, \qquad [6]$$

where N_i^{I} is the cycles-to-crack nucleation at inclusions, N_i^{S} is the cycles-to-crack nucleation at slipbands (*i.e.*, grain facet), ξ is the inclusion size (diameter), and ξ_{o} is the critical inclusion size (diameter) below which there is not fatigue debit due to crack initiation at inclusions. In addition, ξ_{o} serves as a normalizing parameter that links the inclusion-induced crack nucleation life directly to the nucleation life of slipband-induced cracking in the matrix grains. Equation [6] indicates that N_i^{I} decreases with increasing inclusion size according to a power-law once the critical inclusion size is exceeded ($\xi > \xi_{\mathrm{o}}$). Figure 2(a) illustrates the power-law relation between the normalized cycles-to-nucleation at inclusions and the inclusion size normalized by the critical inclusion size. The critical inclusion size is given by

$$\xi_{\mathrm{o}} = 4\pi(1-\nu)(1+\mu/\mu')(h'/h)^4(h/D)h, \qquad [7]$$

where ν is the Poisson's ratio, μ is the shear modulus, D is the grain size (diameter), and h is the slipband width of the matrix; μ' is the shear modulus, and h' is the width of the slipband impinging on the inclusion. It is envisioned that the blocking of a slipband by an inclusion can cause widening of the slipband so that the h'/h ratio is greater than 1. It should also be noted that the critical inclusion size is very sensitive to the h'/h ratio and is proportional to (h'/h) to the 4th power. The inverse relation between the critical inclusion size and

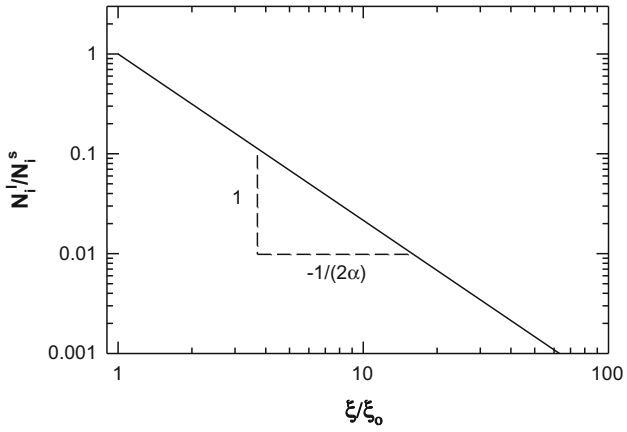

(a)

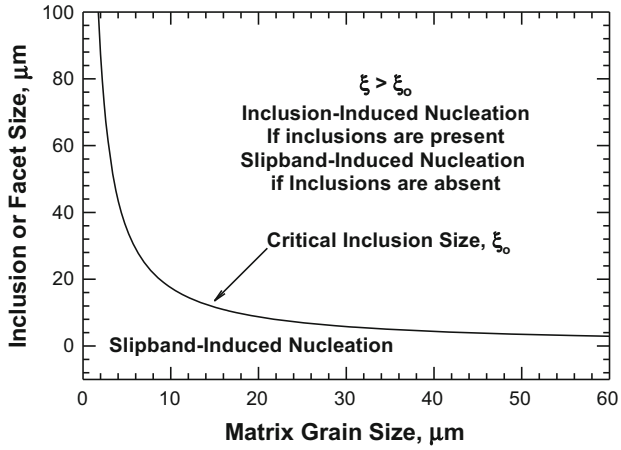

(b)

Fig. 2—(*a*) The scaling of fatigue nucleation life with inclusion size according to a power-law, and (*b*) the scaling of the critical inclusion size with $1/D$ where D is the matrix grain size. Slipband-induced nucleation predominates when $\xi < \xi_o$. Inclusion-induced nucleation predominates when $\xi > \xi_o$ if inclusions of these characteristics are present; otherwise, slipband-induced nucleation prevails.

the matrix grain size is depicted in Figure 2(b). The curve depicts the locus of matrix grain size and inclusion size, where $N_i^S = N_i^I$. As a result, there is an equal chance of slipband nucleation and inclusion-induced nucleation along the locus, being 50 pct chance of occurrence for each mechanism. Below the solid curve ($\xi < \xi_o$), slipband nucleation is the likely crack nucleation mechanism since the cycles-to-nucleation at slipband is less than that of nucleation at inclusions ($N_i^S < N_i^I$). Above the solid curve, $N_i^I = N_i^S$ and inclusion-induced nucleation occurs prior to slipband-induced nucleation if inclusions with sizes larger than ξ_o are present. If these inclusions are not present, then slipband-induced nucleation should prevail since slipband-induced nucleation is taken as the default mechanism.

In addition to fatigue life scaling, a scaling law also exits for the fatigue strength of an alloy with inclusions and without inclusion. The fatigue strength scaling law, which derivation is presented in Appendix, is given by

$$\Delta S_{th}^I = \Delta S_{th}^S \left(\frac{\xi}{\xi_o}\right)^{-1/2}, \quad [8]$$

where ΔS_{th}^I is the fatigue strength with inclusion and ΔS_{th}^S is the fatigue strength of the matrix grains without the presence of inclusions in the microstructure. Equation [8] indicates that the fatigue strength is predicted to decrease with increasing inclusion size according to a power-law with an exponent of $-1/2$, which is slightly higher than the exponent of $-1/3$ observed empirically in steels.[1] For materials with a fatigue limit ($2Mk$), the threshold stress for inclusion-induced crack nucleation can be obtained from Eq. [A4] in Appendix to give

$$\Delta S_{th}^I = 2F_m Mk + \left(\Delta S_{th}^S - 2F_m Mk\right)\left(\frac{\xi}{\xi_o}\right)^{-1/2} \quad [9]$$

which shows the threshold stress for inclusion-induced crack nucleation depends on both the fatigue limit for slipband-induced crack nucleation, the slip process, the inclusion size, as well as the critical inclusion size. Under this circumstance, the scaling of the threshold stress ΔS_{th}^I with the inclusion size may be different from a power-law with the $-1/2$ exponent.

III. EVIDENCE OF CRITICAL INCLUSION SIZE AND FATIGUE LIFE SCALING

Equations [6] and [7] are assessed using experimental data available in the literature, which include a number of powder-metallurgy (PM),[14–22] additively manufactured (AM),[23,24] and forged Ni-based superalloys.[11–13] In particular, Eq. [6] indicates that for inclusion-induced nucleation, the cycles-to-crack nucleation at inclusions decreases with increasing inclusion size according to a power-law. The power-law scaling relation is supported by the experimental data of Zhao *et al.*,[21] who reported the fatigue life of a PM Ni-based superalloy with compositions similar to those of Astroloy.[20] Figure 3(a) shows that the fatigue life of PM Astroloy decreases with increasing inclusion size according to a power-law as suggested by Eq. [6]. Pertinent model constants for N_i^S and α were determined and are presented in Figure 3(a). The inclusion size studied by Zhao *et al.*[21] ranged from 20 to 100 μm, but the grain size was not reported. Consequently, literature data from other sources[20] were used to compare against the predicted critical inclusion size. The material parameters in Eq. [7] include shear moduli of the inclusion and the matrix, the slipband width (h') impinging on the inclusions, the slipband width (h) within the matrix grains, and the matrix grain size in the Ni-based superalloy. The slipband width for various superalloys were compared and are summarized in Table I.[45–55] Young's moduli of Al_2O_3, NbC, and Ni compiled by Chan[56] were used to compute the shear moduli of these inclusions and the superalloy matrix. The shear moduli of Al_2O_3 and NbC are similar (1.28E + 5 MPa) and the shear modulus of Ni is about 7.04E + 4 MPa. A

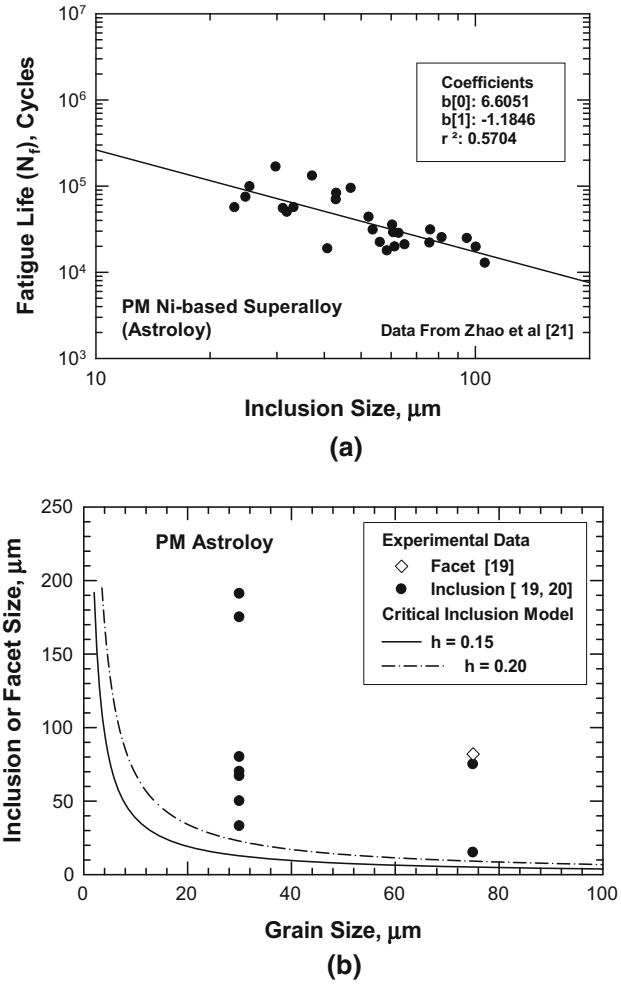

Fig. 3—(*a*) Power-law relation between fatigue life and inclusion size observed in a PM Ni-based superalloy with compositions similar to Astroloy, and (*b*) Inclusion and facet size *vs* grain size compared to the calculated critical inclusion size for PM Astroloy. Experimental data are from the literature.[19,20]

summary of the model constants used in conjunction with Eq. [7] to compute the critical inclusion size is presented in Table II. The predicted critical inclusion size for Astroloy is presented in Figure 3(b). The predicted curves lie below the experimental data for Astroloy because the inclusions in the Astroloy materials were seeded by large inclusion particles in order to ensure early failure. As a consequence, most of the inclusions exceeded the critical inclusion size and with the exception of one data point, the fatigue cracks nucleated from large inclusions, as shown in Figure 3(b).

The existence of a critical inclusion size that depends on the matrix grain size in PM Rene 95 and Rene 88DT is illustrated in Figure 4. Fatigue cracks nucleated at non-metallic inclusions (NMI) and oxide (Al_2O_3) particles in these two alloys. A comparison of the model prediction against the experimental data of Rene 95 indicates good agreement and the critical inclusion model appears to be valid for Rene 95. Since N_i^{I} is identical to N_i^{S} for nucleation at slipbands when $\xi = \xi_o$, a possible means of identifying $\xi = \xi_o$ is the concurrent presence of slipband facets and inclusion nucleation sites on the same fatigue fracture surfaces, as observed in PM Rene 88DT in Figure 4. At a grain size of 30 μm, only inclusion-induced nucleation was observed at inclusion sizes larger than the critical inclusion size, in agreement with the model. However, both inclusion-induced and slipband-induced nucleation modes were observed at a grain size of 25 μm. The observation of faceted nucleation above the critical inclusion size curve suggests that other factors may be important. One possibility is that large inclusions may not be present or they are more resistant to crack nucleation than that postulated in the current model. At this time, these two possibilities are feasible and cannot be discerned because of a lack of information on the inclusion size distribution. In a LCF life study of Rene 88DT seeded with inclusions, Huron and Roth[37] reported that the crack nucleation life of

Table I. Summary of Slipband Width in Nickel Alloys

Alloy	T [K (°C)]	Grain Size (μm)	Slipband Width (μm)	Technique	References
Pure Ni	RT	80	0.7	SEM	Weidner *et al.*[45]
	RT	80	0.7	AFM	Weidner *et al.*[46]
			0.9	SEM	
	RT	80	0.07 to 0.08	SEM	Weidner *et al.*[47]
Ni 200	RT	70	0.5	SEM	Chan *et al.*[51]
			(0.3 to 1)		
Waspaloy	RT	30	0.08	SEM/AFM	Risbet *et al.*[50]
	RT	50	0.121 to 0.171	AFM	Ho *et al.*[55]
		100	0.13 to 0.15		
KM4	RT	55	0.04	TEM	Shyam and Milligan[52]
			0.02 to 0.06	TEM	
			0.07 to 0.14	Optical	
ME3	977 (704 °C)	44	0.3	SEM	Dahal *et al.*[54]
	1033 (760 °C)		0.6	SEM	
CMSX-4	973 (700 °C)	0.5 $(\gamma')^+$	0.13 to 0.16	TEM	Obrtlik *et al.*[49]
	973 (700 °C)	0.5 $(\gamma')^+$	0.13	TEM	Lukas and Kunz[48]
Superalloy SX (IN792 or PWA 1483)	1033 (760 °C)	0.25 $(\gamma')^+$	0.1 (in γ)	TEM	Zhang *et al.*[53]
			0.085 (in γ')	TEM	

$^+\gamma'$ size.

seeded specimens decreases with increasing inclusion size according to a power-law of the form shown in Eq. [6]. For specimens tested at 477K (204 °C), 80 pct of the test specimens nucleated fatigue cracks at grain facets. In contrast, 98.7 pct of the specimens tested at 922K (649 °C) exhibited crack nucleated at inclusions.

Figures 5(a) and (b) evaluate the validity of Eq. [7] to determine the potential existence of a critical inclusion size in forged IN 718, where fatigue cracks nucleated at carbides. A summary of the model constants for computing the critical inclusion size is presented in Table II. One possible way of assessing Eq. [7] is to plot the inclusion size where fatigue crack is nucleated as a function of the matrix grain size. Figure 5(a) presents the inclusion (carbide) size as a function of the grain size in a log–log plot for carbide-induced and slipband-induced fatigue crack nucleation in IN 718. The data points for carbide-induced nucleation fall within a small band exhibiting decreasing inclusion size with increasing matrix grain size, in accord with Eq. [7]. The experimental data within the small band were fitted to Eq. [7]. Most of the material constants are known with the exception of h'. As a result, three different values of the h'/h ratio were used to fit the model, Eq. [7], to the experimental data, as shown in Figure 5(a). The experimental data for IN 718 appear to support the model prediction that the critical inclusion size is proportional to $1/D$, where D is the grain size of the matrix. Equation [7] was used to compute the critical inclusion size as a function of matrix grain size and the results are compared with the experimental data of IN 718,[11–13] IN 718DA[40–42] and GH4169[43,44] in Figure 5(b). The comparison shows that the critical inclusion size increases rapidly with decreasing matrix grain size. Furthermore, the model predicts correctly slip-induced crack nucleation at larger grains (30 μm[42] and 48 μm[43]), as shown in Figure 5(b). Crack nucleation in grains as large as 83 μm[43] has also been reported, even though it is not shown in Figure 5(b). In addition, the model prediction of increasing critical inclusion size at decreasing grain size is supported by the experimental data for IN 718, IN 718DA, and GH4169. In particular, Texier *et al.*[40,41] reported that in IN 718DA with a fine-grained microstructure (12 to 13 μm mean size and 25 μm maximum size) containing small inclusions (4 to 5 μm mean and 25 μm maximum size), fatigue crack nucleation occurred at carbide clusters (31 to 33 μm) or at small carbide inclusions (12 to 13 μm), but switched to slipband-induced crack nucleation in larger grains (22 to 26.8 μm). Similarly, Deng *et al.*[44] reported inclusion-induced nucleation in GH4169 with a small mean grain size (9 μm), but the crack nucleation process switched to grain boundary nucleation in material with a larger mean grain size (25 μm). The inclusion size in the GH4169 material ranged from 4 to 10 μm.[44] These observations are in agreement with the model predictions shown in Figure 5(b). The carbide clusters reported by Texier *et al.*[40,41] are substantially larger than the critical size for inclusion-induced crack nucleation. Crack nucleation at the carbide clusters was indeed observed.[40,41] In contrast, slip-induced crack nucleation was observed in IN 718[11] for a range of grain sizes where carbide-induced nucleation are expected. The lack of carbide-induced nucleation in these cases may be attributed to the absence of large carbides in excess of the critical inclusion size in these grains. The inclusion size and grain size distributions reported by Texier *et al.*[40,41] and by Abikchi *et al.*[42] for IN 718DA indicated that a combination of large grains (25 μm) and large carbides (25 μm) is rare and the feature sizes are near the right tails of the individual distributions. Figure 5(b) indicates that for IN 718, IN 718DA, and GH4169, slipband-induced nucleation predominates at larger grain sizes (> 25 μm) because of the absence of large carbides (> 25 μm). The propensity of carbide nucleation increases in a fine-grained microstructure even though the critical inclusion size increases with decreasing grain size. In addition, inclusion-induced nucleation is seen to be enhanced by the presence of carbide clusters.

Like PM and forged Ni-based superalloys, the critical inclusion model appears to be applicable to AM 718Plus. Figure 6 presents application of the critical inclusion size model to AM 718Plus for the fully machined condition tested in the build direction. The as-built specimens were not considered since the rough surfaces contain notch-like features that can serve as fatigue crack nucleation sites. Fractographic evidence indicated the presence of slipband facets and oxide-induced nucleation sites in fully machined AM 718Plus LCF specimens. The inclusions in AM 718Plus are NMI and oxide particles. These inclusion-induced nucleation sites are mixed with crack nucleation at facets. The inclusion sizes were slightly larger than critical inclusion sizes, as shown in Figure 6. The grain size of the AM material is about 20 μm in the build direction but is about 70 μm in the scan direction, which is aligned normal to the stress direction.

Another implication of Eq. [6] is that the S–N_f curve for inclusion-induced nucleation may be comparable to that for nucleation at slipbands when $\xi = \xi_o$. Experimental evidence for this model prediction can be found in the S–N_f curve of PM ME3 with the supersolvus microstructure. Figure 7 presents a comparison of the stress–fatigue life (S–N_f) curves computed based on the slipband nucleation model, Eq. [1], and the inclusion-induced nucleation model, Eq. [4]. As shown in Figure 7, the S–N_f curves for the two crack nucleation models are comparable and both are supported by experimental observations of fracture facets and inclusion-induced nucleation in the respective LCF specimens. Figure 7 also shows that there are considerable scatter in the LCF lives. A further comparison of the model predictions and experimental data might arise from a variation in the fatigue limit, as shown in Figure 8. The variation in the fatigue limit may be the consequence of possible difference in the inclusion size, ξ, the γ' size and the distribution of γ', the friction stress, k, for slip, and the Taylor factor, M, which depends on the local texture of matrix grains.

Table II. Summary of Model Constants for Computing the Critical Inclusion Size for Selected Ni-Based Superalloys

Alloy	Inclusion Type	μ (MPa)	μ' (MPa)	h (μm)	h'/h
Astroloy	oxide	7.04E+04	1.28E+05	0.15 to 0.20	6
AM 718Plus	NMI + oxide	7.04E+04	1.28E+05	0.1	7.5
IN 718	carbides	7.07E+04	1.28E+05	0.1	5.75
Rene 95	NMI + oxide	7.07E+04	1.28E+05	0.17	6
Rene 88DT	NMI + oxide	7.07E+04	1.28E+05	0.2	6
ME3	NMI	7.07E+04	1.28E+05	0.1 to 0.3	6

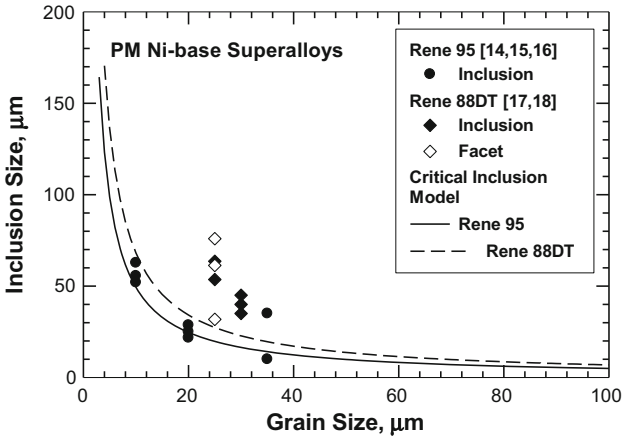

Fig. 4—The existence of a critical inclusion size and its dependence on grain size observed in Rene 95[14–16] and Rene 88DT[17,18] in which fatigue cracks nucleated at NMI and oxide (Al_2O_3) particles.

IV. DISCUSSION

To put the results of this investigation into proper perspective, it is instructive to discuss the dependence of fatigue nucleation life on grain size and inclusion size and to elucidate the origin of the critical inclusion size. According to Eqs. [1] and [2], the slip-induced nucleation life, N_i^S, can be expressed in term of the grain size as

$$N_i^S = g_1(\mu, \sigma_a, M, k)\left(\frac{h}{D}\right)^{1/\alpha} \quad [10]$$

$$\text{with } g_1(\mu, \sigma_a, M, k) = \left(\frac{2\sigma_a}{F_m} - 2Mk\right)^{-1/\alpha}\left[\frac{8M^2\mu^2}{\lambda'\pi(1-\nu)}\right]^{1/2\alpha}, \quad [11]$$

where $g_1(\mu, \sigma_a, M, k)$ represents function of μ, σ_a, M, and k but not grain size, when the pile-up length (or crack length) $2c$ is taken to be the grain size (*i.e.*, $2c = D$). For a given stress amplitude and constant h, N_i^S increases with decreasing grain size according to the $(h/D)^{1/2\alpha}$ dependence. For Ni-based superalloys containing inclusions, the inclusion-induced nucleation life, according to Eqs. [3] and [4], is given by

$$N_i^I = g_2(\mu, \mu', \sigma_a, M, k, h'/h)\left(\frac{h}{D}\right)^{2/\alpha}\left(\frac{D}{\xi}\right)^{1/2\alpha} \quad [12]$$

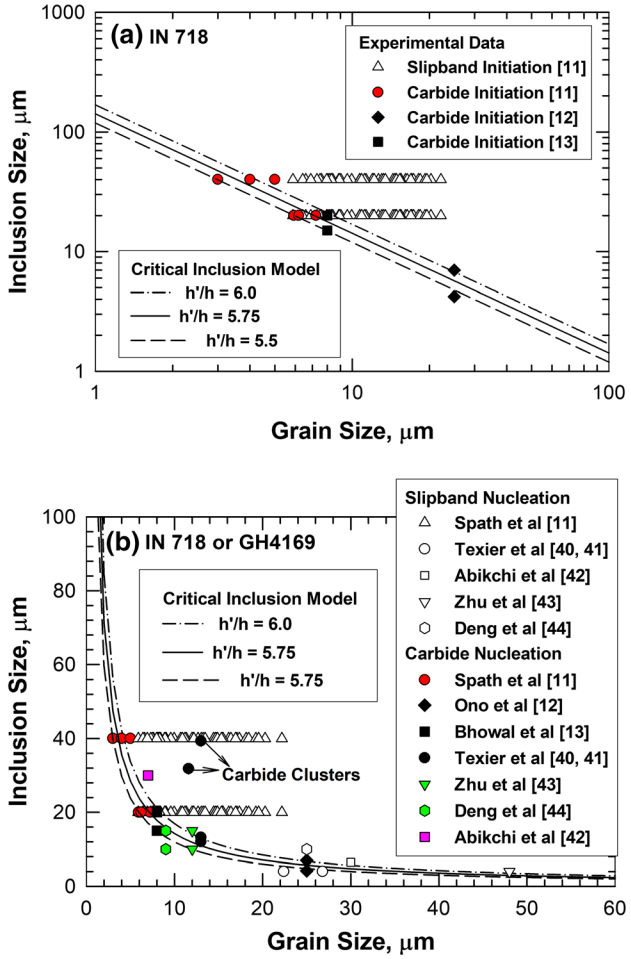

Fig. 5—The existence of a critical inclusion size and its dependence on grain size observed in IN 718,[11–13] IN 718DA,[40–42] and GH4169[43,44] in which fatigue cracks nucleated at carbide particles (filled symbols) or slipbands (open symbols): (*a*) inclusion size *vs* grain size in a double logarithmic plot, and (*b*) inclusion size *vs* grain size in a linear plot.

when $2c$ is taken to be the grain size D. Equation [12] can be rewritten as

$$N_i^I = N_i^*\left(\frac{D}{\xi}\right)^{1/2\alpha} \quad [13]$$

$$\text{with } N_i^* = g_2(\mu, \mu', \sigma_a, M, k, h'/h)\left(\frac{h}{D}\right)^{2/\alpha} \quad [14]$$

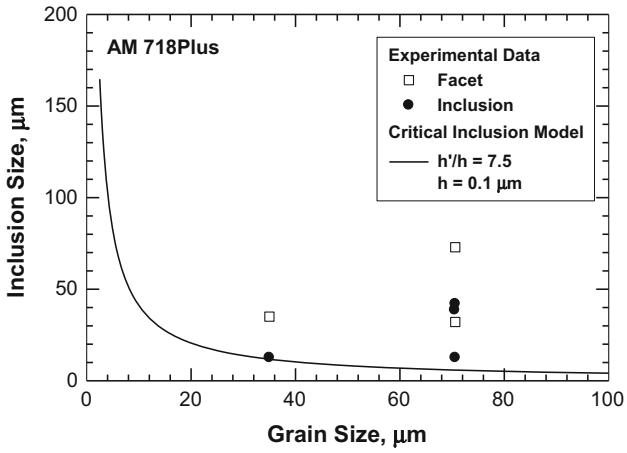

Fig. 6—Observed crack nucleation sites compared to the critical inclusion model for AM 718Plus[23,24] with fully machined surfaces.

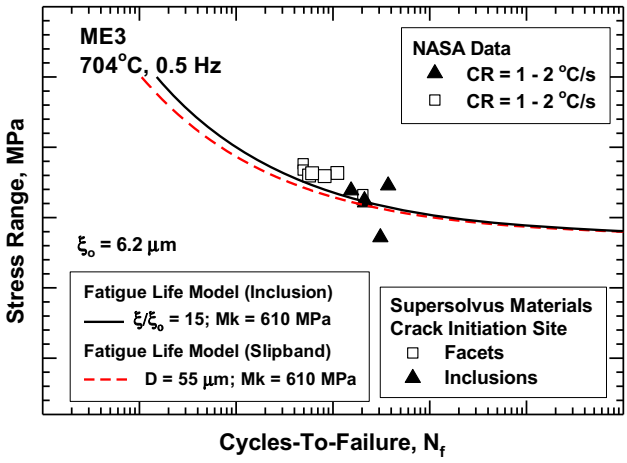

Fig. 7—Comparison of S–N_f Curves of ME3 exhibiting slipband-induced nucleation and inclusion-induced nucleation against model predictions based on slipband-induced nucleation, Eq. [1], and inclusion-induced nucleation, Eq. [4]. Experimental data are from Gabb *et al.*[22] *CR* cooling rate.

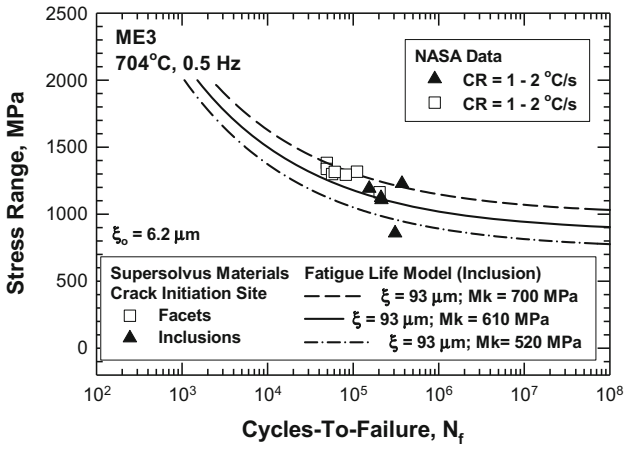

Fig. 8—S–N_f Curves of ME3 computed based on different fatigue limits (Mk) compared against experimental data from Gabb *et al.*[22]

$$\text{and } g_2 = \left[4\pi(1-\nu)(1+\mu'/\mu)(h'/h)^4\right]^{1/(2\alpha)} g_1(\mu, \sigma_a, M, k) \quad [15]$$

Equation [14] indicates that N_i^* is function of grain size and other material parameters, but is not function of the inclusion size. From Eq. [13], it is apparent that N_i^I decreases with increasing inclusion size. In addition, $N_i^I \geq N_i^*$ when $D \geq \xi$. In contrast, $N_i^I \leq N_i^*$ when $\xi \geq D$. When the matrix grain size is decreased, N_i^*increases by virtue of its dependence on $\left(\frac{h}{D}\right)^{2/\alpha}$ (Eq. [14]) while the $\left(\frac{D}{\xi}\right)^{1/2\alpha}$ term is reduced. Thus, the N_i^I value, Eq. [12], may increase or decrease due to the opposite dependence of N_i^* and $\left(\frac{D}{\xi}\right)^{1/2\alpha}$ on grain size. A closer inspection of Eq. [12] indicates that N_i^I is likely to increase with decreasing grain size until it is prevented from further increases by the reduction of the $\left(\frac{D}{\xi}\right)^{1/2\alpha}$ term. At a certain small grain size or inclusion size, $N_i^I < N_i^*$, and crack nucleation occurs at inclusions rather than at slipbands. Equations [12] and [13] were utilized to illustrate the effects of grain size and inclusion size on crack nucleation mechanisms by computing N_i^I and N_i^* as a function of grain size (D) for inclusion sizes ranging from 20 to 200 μm. For these computations, g_2 was arbitrarily taken to be 1.0E + 10 cycles so that details of the crack nucleation transitions can be depicted clearly. The results of these computations are presented in Figures 9(a) and (b) for inclusion sizes of 50 μm and 20 μm, respectively. Figure 9(a) shows that N_i^I and N_i^* decrease at different rates while the $\left(\frac{D}{\xi}\right)^{1/2\alpha}$ term increases with increasing grain size. The computed N_i^I curve intersects and crosses the N_i^* curve at $N_i^I = N_i^*$ and $\xi = D$. At $D > \xi$, the N_i^* curve lies below the N_i^I curve, indicating that slip-induced nucleation with facet formation is the favored fatigue mechanism. In contrast, the N_i^I curve lies below the N_i^* curve and the fatigue mechanism switches from facet formation to inclusion-induced nucleation when $D < \xi$. Thus, the model predicts a transition of facet formation at large grains to inclusion-induced nucleation at small grain sizes. Figure 9(b) shows that similar transition of fracture modes occurs when the inclusion size is taken to be 20 μm. The results for inclusion size 100 and 200 μm are also similar to those of 50 μm, but the transition points are shifted to the larger grain sizes with lower fatigue lives. In all cases, the computed N_i^I curve intersects and crosses the N_i^* curve at $N_i^I = N_i^*$ and at $\xi = D$. In addition, the curves show a transition of facet formation at large grains to inclusion-induced nucleation at grains sizes that are smaller than the imposed inclusion sizes. The transition arises from increases in the N_i^* due to higher resistance to slipband nucleation with decreasing grain sizes. It is also important to note that in all cases considered, the transition point corresponds to the point of equal values of nucleation lives ($N_i^I = N_i^*$) for the two competing mechanisms. The occurrence of concurrent

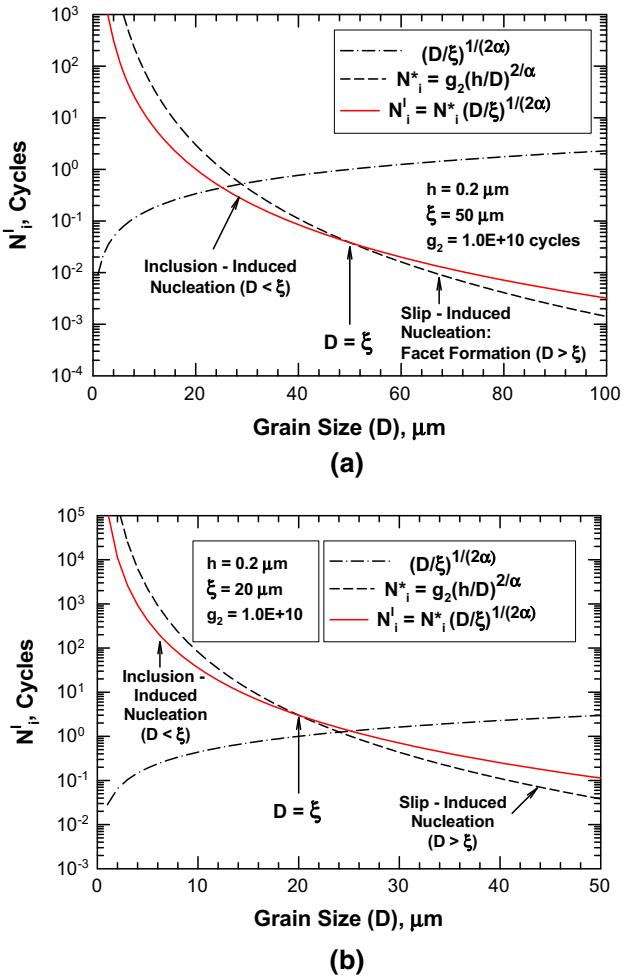

Fig. 9—Computed inclusion nucleation life curve (N_i^I) and slip-induced nucleation life curve (N_i^*) as a function of grain size for two inclusion sizes: (*a*) $\xi = 50$ μm, and (*b*) $\xi = 20$ μm. For both cases, the nucleation life curves crossover each other at $D = \xi$. Slip-induced nucleation is favored when $D > \xi$, while inclusion-induced nucleation is favored when $D < \xi$.

inclusion-induced nucleation and facet formation, shown in Figure 7 for ME3, is an indication that the inclusion size and the grain size are near or at the transition point.

From Figure 9, it is obvious that the proposed models (Eqs. [12] through [14]) predict the dominance of slip-induced nucleation and facet formation in large-grained materials and a transition from slipband nucleation and facet formation to inclusion-induced nucleation when the grain size is reduced. In addition, the results also show clearly that for materials containing inclusions with a size on the order of the mean grain size, the as-large-as (ALA) grains are expected to promote slipband nucleation and facet formation since the ALA grains are always larger than the mean grain size. The predicted crack nucleation behaviors are in agreement with experimental data of IN 718 shown in Figure 5. The predicted behaviors are also supported by the findings of Gabb *et al.*,[57,58] who reported that facet formation was the dominant fatigue crack nucleation mechanism in the supersolvus region of a LSHR disk where the grain size was relatively large (55 μm mean and 150 to 400 μm ALA grain size) and the transition of facet formation to inclusion-induced nucleation in the subsolvus region where the grain size was small (5 to 10 μm). Gabb *et al.*[57,58] also reported that the fatigue facets in the supersolvus materials, which occurred at ALA grains, ranged from 150 to 400 μm. The inclusion size in LSHR was about 19 to 50 μm (see Figure 5 in Gabb *et al.*[57] and Table I in Gabb *et al.*[58]). Based on the results in Figure 9, it can be expected that slip-induced crack nucleation and facet formation occur at the large ALA grains in the supersolvus microstructure and a transition from facet formation to inclusion-induced nucleation occurs when the grain size is reduced to 5 to 10 μm in the subsolvus microstructure. This type of fracture mechanism transition is expected to be prevalent in materials that are heat-treated to exhibit dual microstructures of large-grained and small-grained regions such as those obtained by dual microstructure heat treat (DMHT) procedures.[57,58]

Equation [12] indicates that besides grain size and inclusion size, other material parameters such as inclusion properties and slip morphology in the matrix may also play a role in the transition of crack nucleation mechanisms. The LCF model developed in this investigation was intended to relate explicitly the nucleation life to the microstructural feature sizes and material parameters that control the transition of slip-induced nucleation to inclusion-induced nucleation by taking into account of inclusion size, grain size, inclusion properties, and slip morphology in the matrix grains. A systematic evaluation of the transition point, which is the crossover point of the N_i^I curve and the N_i^* curve, indicates that the transition always occurs at $N_i^I = N_i^*$ and at $\xi = D$. Figure 10(a) shows that the locus of the transition curve is a 45 deg line in a plot of inclusion size *vs* grain size in a linear scale. The slip-induced nucleation region is located below the $N_i^I = N_i^*$ and $\xi = D$ line. In this region, the grain size is larger than the inclusion size ($D > \xi$) as shown in Figure 9. In contrast, the inclusion-induced nucleation region resides above the $N_i^I = N_i^*$ and $\xi = D$ line. In this region, the grain size is smaller than the inclusion size ($D < \xi$), as shown in Figure 9. The condition of $\xi = D$ is not an adequate or insightful criterion for use as the transition of slip-induced nucleation to inclusion-induced nucleation since the influence of matrix slip morphology and inclusion properties have not been included. After these material parameters are incorporated, the transition point does not occur at $D = \xi$, but occurs at the critical inclusion size, as defined in Eq. [7], under equal life conditions ($N_i^I = N_i^*$) at the competing nucleation sites. The transition criterion is preferred because it explicitly includes the $1/D$ dependence of the slip process that has been identified from previous studies[5,6,10,11,15] and it leads to a simple scaling law, Eq. [6], for describing the effects of inclusion size on nucleation life. By incorporating the $1/D$ dependence in the definition of the critical inclusion size, the transition curve is now a function of grain size as shown in Figure 10(b). The slip-induced nucleation region is now located below the transition

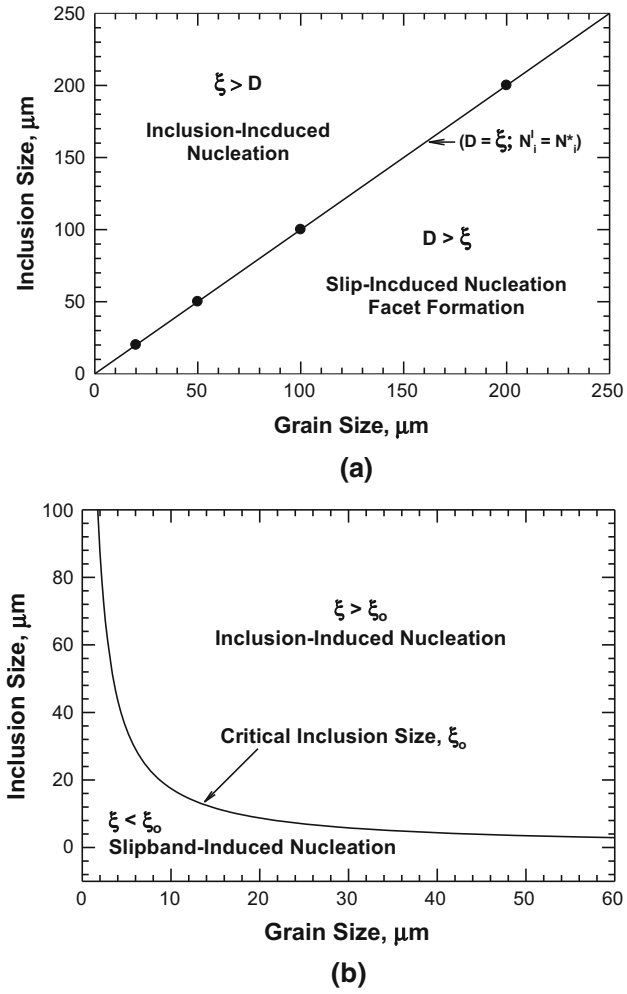

Fig. 10—A comparison of the transition criterion based on equal size or equal nucleation life: (*a*) equal inclusion and grains size without accounting for other material parameters, and (*b*) equal nucleation lives at competing nucleation sites based on the critical inclusion sizes and other contributing material parameters as defined in Eq. [7].

curve as the $D > \xi$ criterion in Figure 10(a) becomes $\xi < \xi_o$ in Figure 10(b) because D transforms to $1/D$ in the conversion process. Similarly, the inclusion-induced region in Figure 10(a) remains located above the transition curve in Figure 10(b). In this region, $\xi > \xi_o$. Figure 10(b) is essentially identical to that shown in Figure 2(b), which includes the stipulation that inclusions must be present in the inclusion-induced nucleation region. The critical inclusion size serves as the normalizing parameter that collapses the N_i^I curve and the N_i^* curve on top of each other (as shown in Figure 7 for ME3) so that the inclusion-induced nucleation life scales with the inclusion size as described in Eq. [6] without the need to have a full knowledge of the size distribution of the matrix grains.

The important findings of this investigation include (1) a scaling law between crack nucleation life and inclusion size, (2) the existence of a critical inclusion size below which there is no fatigue life debit, and (3) a set of scaling laws for the threshold stress range for fatigue

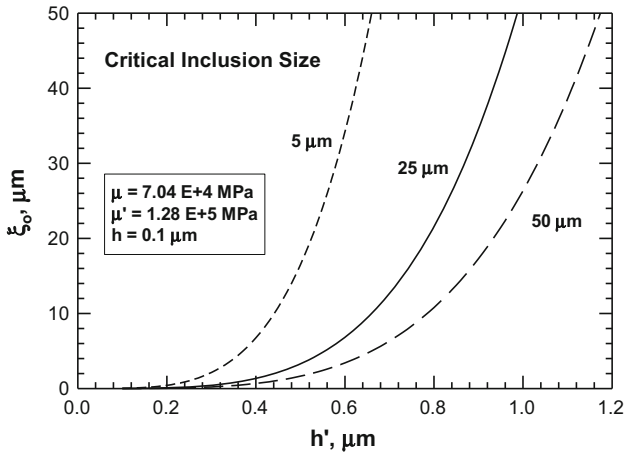

Fig. 11—Critical inclusion size as a function of the slipband width, h', impinging at inclusions by slip in matrix grains of various grain size.

crack nucleation. The scaling law has been obtained by incorporating the $1/D$ grain size dependence explicitly in the definition of the critical inclusion size. The consequence is that slip-induced nucleation occurs when $\xi < \xi_o$ (from $D > \xi$, see Figure 9) and inclusion-induced nucleation when $\xi > \xi_o$ (from $D < \xi$, see Figure 9) due to the incorporation of $1/D$ in the definition of ξ_o (see Eq. [7]). The experimental data in the literature[21,37] provide strong support for the notion that the fatigue nucleation life of PM Ni-based superalloy decreases with increasing inclusion size according to a power-law as indicated in Eq. [6]. Experimental data in the literature also support the existence of a critical inclusion size below which the fatigue nucleation life is not affected by or insensitive to the inclusion size. From Eq. [7], it is apparent that the critical inclusion size increases with the ratio of h'/h according to a power of 4 and increases with decreasing matrix grain size. In contrast, the critical inclusion size is only mildly dependent on the shear modulus of the inclusion. Figure 11 illustrates the dependence of the critical inclusion size on the slipband width (h') impinging on inclusions calculated *via* Eq. [7] using material constants for ME3. The results in Figure 11 show that the critical inclusion size increases rapidly with increasing values of h'. Thus, slipband widening by an inclusion can have a positive and important effect in increasing the critical inclusion size. In addition, the critical inclusion size increases with decreasing matrix grain size, as shown in Figure 11. The values of slipband width, h, in matrix grains of Ni-based superalloys have been compiled and are summarized in Table I. Unfortunately, the value for h' is generally not reported in the literature. For model calculations presented in this article, h is taken to be 0.1 to 0.2 μm and the ratio h'/h is taken to be about 5.5 to 7.5. This range of h'/h values leads to h' values of 0.6 to 1.0 μm when h is taken to 0.1 μm, which is within the variation of h values compiled in Table I. Additional work is required to confirm this range of h'/h values for Ni-based superalloys.

It is apparent that the slip process in the matrix (γ) grains exerts a significant influence on the crack nucleation mechanism in Ni-based superalloys. In general, shearing of γ' by dislocation pairs tends to localize slip and form narrow slipband width.[59] Widening of slipbands requires cross-slip of superdislocations with superkinks.[59] Non-shearable particles such as non-metallic inclusions, on the other hand, force the dislocations to bow around and bypass the obstacles,[59] which can result in the formation of geometrically necessary dislocations (GND) at the matrix/inclusion interface and lead to crack formation at slipbands, inclusions, or at matrix/inclusion interface.[34–36] Using high-resolution electron backscatter diffraction, Jiang *et al.*[34] showed that an increase in cyclic hardening is manifested by increasing GND density and the formation of a GND network around a non-metallic inclusion during low-cycle fatigue of a PM Ni-based alloy. Thus, there is experimental support for the widening of a slipband that impinges on a non-metallic inclusion. The widening of the slipband width, h', by GND density can potentially increase the critical inclusion size and make crack nucleation at inclusions more difficult to occur. The test temperature has also been reported to affect slip morphology in grains and the fatigue properties of carbides such that the relative percentages of facet and inclusion-induced nucleation vary with temperature, inclusion type, and alloys.[13,37]

It is envisioned that the fatigue crack nucleation life at an inclusion can be predicted based on Eq. [6] once the critical inclusion size is computed on the basis of Eq. [7]. As shown in Figure 12, the normalized fatigue nucleation life scales with the critical inclusion size, with increasing fatigue life ratio at a larger inclusion size when the critical inclusion size is increased. Both the power-law scaling law and the existence of a critical inclusion size were previously reported for steels based on experimental observations and fitting of experimental data.[60,61] For steels, the critical inclusion size was reported to be around 15 to 20 μm.[60–63] The exponent of the fatigue strength scaling law, Eq. [8], is predicted to be $-1/2$, which is slightly higher than the experimental value of $-1/3$ observed in steels.[1,62] The discrepancy

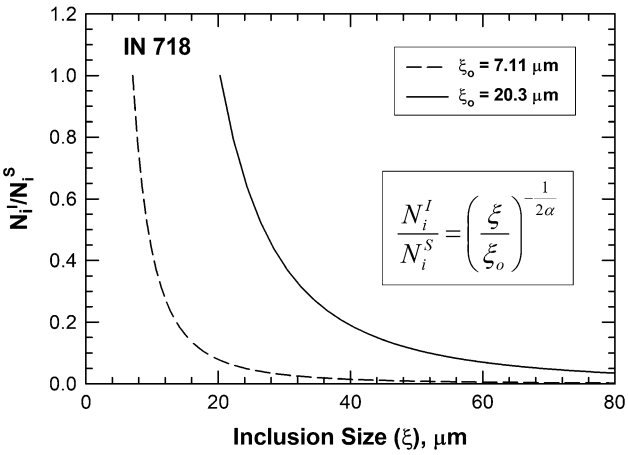

Fig. 12—Fatigue life prediction of inclusion-induced crack nucleation based on inclusion size scaling.

may be attributed to the fact that the 2Mk values for steels may not be small to be ignored and Eq, (9) should be used in the data analysis in order to obtain the correct dependence. The applicability of Eq. [8] to Ni-based superalloys remains an open question since a detailed comparison and evaluation of Eq. [8] against experimental data has yet to be made.

Once the fatigue crack is formed, the inclusion-sized crack can be checked to determine whether or not the corresponding ΔK has exceeded the large-crack threshold in order to compute the corresponding da/dN response, as shown in Figure 13, which shows the threshold stress regimes for (1) crack nucleation at inclusion, (2) non-propagating cracks, and (3) large-crack growth to failure. In Figure 13, the solid curve for crack nucleation is computed based on Eq. [8], while the dashed curve for the threshold stress for crack growth is based on a modification of the worst-case notch analysis by Hudak *et al.*[64] through replacing the crack depth with one-half of the inclusion diameter and assuming the entire inclusion is cracked to form a crack length of $2a = \xi$. The resulting equation for the worst-case inclusion analysis is shown as an inset in Figure 13 and the dashed curve is computed based on $\Delta K_{th} = 3$ MPa(m)$^{1/2}$, $\Delta\sigma_e = 482$ MPa, $\xi_o = 20.3$ μm, and $a_o = 38.5$ μm, where ΔK_{th} is the large-crack threshold, $\Delta\sigma_e = 2$Mk is the fatigue limit in the absence of inclusions, and a_o is the small-crack parameter of El Haddad el al.[65] At stress ranges above threshold stress range for crack nucleation, fatigue crack nucleation at inclusion can occur, but the nucleated crack may not propagate. At stress ranges above the threshold stress intensity factor for large-crack growth, the nucleated microcrack can propagate to become a large crack and cause ultimate fracture at the critical stress intensity for fracture. It should also be noted that at stress ranges within the non-propagation regime, microcrack nucleation at inclusion can proceed and the non-propagating microcrack can coalesce to become a larger microcrack to allow its further growth when the large-crack threshold is exceeded at the tip of the microcrack.

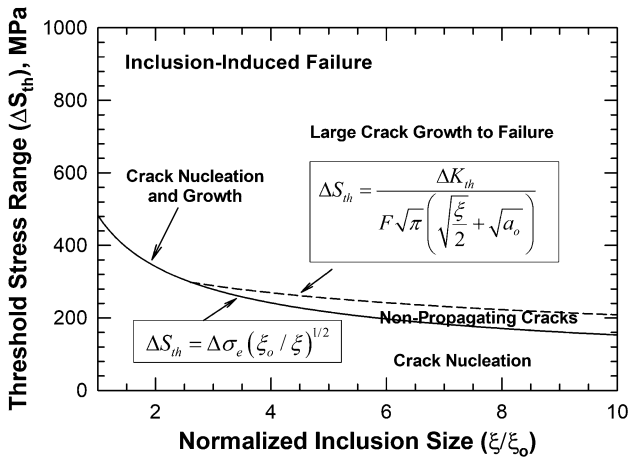

Fig. 13—Fatigue mechanism map for AM 718Plus with fully machined surfaces depicting three fatigue failure regimes (1) crack nucleation at inclusion, (2) non-propagating cracks, and (3) large-crack growth to failure.

Figure 13 shows that the threshold stresses for crack nucleation and crack growth both decrease with increasing inclusion size. In addition, the regime for non-propagating inclusion crack is relatively small for this particular value of ΔK_{th} of 3 MPa(m)$^{1/2}$. The non-propagation regime is increased by a higher ΔK_{th} or reduced to zero by a lower ΔK_{th} value. At $\xi/\xi_o < 2.5$, fatigue cracks nucleate and propagate to become large cracks without any arrest or non-propagation behaviors. At $\xi/\xi_o > 2.5$, the nucleated inclusion cracks can arrest without further propagation. Under this circumstance, the nucleated inclusion-induced fatigue cracks are controlled by the threshold stress for crack growth. Successful applications of the crack nucleation models[29,30] for treating crack nucleation in IN718 under loading in the very high cycle fatigue regime were reported by Ma *et al.*[66] The concept of a critical inclusion size for crack nucleation at inclusions is useful and has practical applications in processing control since the processing cost may be reduced if a tight control of the inclusion size can be relaxed.[67]

From the discussion above, it is apparent that a critical inclusion size can originate from the crack nucleation or crack growth process. The current model is based on crack nucleation as the limiting process, while the model by Murakami *et al.*[32,33] is based on the growth of microcracks nucleated at inclusions as the limiting process. As such, the present model is not applicable for materials containing inclusions that are initially cracked or highly irregular inclusions that fracture in a few cycles due to localized stress and strain concentrations. Under these circumstances, the crack nucleation life is negligible and the fatigue life is dominated by fatigue crack growth. The existence of a crack nucleation or incubation period late in the fatigue life of PM Ni-based superalloys has been reported by Huron and Roth[37] for Rene 88DT tested at 477 K and 923K. In addition, the observations of nucleation-dominated and growth-dominated fatigue fracture in Ni-based superalloys have been reported in recent studies.[17,26,40–44] Depending on the critical inclusion size and the matrix grain size, slipband nucleation and inclusion nucleation can occur concurrently, leading to substantial variations in the fatigue lives.[17,26,40–44,57,58] The variability in the fatigue life of Ni-based superalloys arises from variations in the fatigue mechanism (nucleation- or growth-dominated process), fracture mode (slipband-induced or inclusion-induced), microstructure (such as grain size and inclusion size), shearing of the ordered precipitates and their distributions (γ' and γ'' in the case of IN 718 and GH4139), dislocation structure (dislocation pile-up or GND), air *vs* vacuum environments,[25] and the hardening response of slipbands impinging on the inclusions. Some, if not all, of these factors may have contributed to the large variations in fatigue life observed in Ni-based superalloys[17,26,40–44,57,58] and in steels.[68] Since the microstructure and dislocation structure affect the crack nucleation and crack growth processes differently, the probability of crack nucleation is therefore quite different from the probability of a crack propagating to fracture; these differences, in turn, lead a large variation in fatigue lives.

It should be noted that in the absence of pores or eligible inclusions, the crack nucleation mechanism in Ni-based superalloys is slipband cracking due to the propensity of shearing of ordered precipitates (γ' or γ'') and planar slip in these alloys. Slip-induced nucleation with facet formation is seen to occur in the region where the critical inclusion size is exceeded, *e.g.*, Rene 88DT (Figure 4), IN 718 (Figure 5), and AM 718Plus (Figure 6). The observation of concurrent slip-induced and inclusion-induced nucleation, which does not necessarily invalidate the current model, may be rationalized on the basis of occurrence rates of individual anomalies in these alloys. As indicated earlier, the location, type, size, number density, and occurrence rate of anomalies such as pores and inclusions are important factors that can affect the risk of fatigue fracture of Ni-based superalloys.[39] The results of this investigation indicate that the effects of grain size should also be considered in conjunction with pores and inclusions as one of the potential sites for fatigue crack nucleation to take place in PM Ni-based superalloys. The probability of fracture, P_F, of a material containing multiple anomalies (pores, inclusions, and large grains) at multiple locations is given by[39]

$$P_F = 1 - \prod_{i=1}^{m} \exp[-\lambda_i V_i P(F_i|d_1)], \qquad [16]$$

where m is the number of anomalies considered, λ_i is the occurrence rate of an anomaly (in average number per unit volume), V_i is the volume at location i, and $P(F_i|d_1)$ is the conditional probability of fatigue fracture given the presence of a single anomaly of size d_1. Ni-based superalloys are typically HiPP'ed at elevated temperatures to eliminate any porosity present in the materials. If the occurrence rate of porosity is reduced to zero by HiPP'ing, the probability of fracture due to crack nucleation at pores is then zero. Similarly, if a material is processed to eliminate large inclusions, large carbides, and large grains from the microstructure, fatigue crack nucleation at these anomalies would be reduced accordingly; the crack nucleation process would then shift to take place at small carbides or inclusions that exceed the critical size or at larger grains near the maximum limit of the grain size distribution of the fine-grained materials. This scenario appears to be the case associated with fatigue crack nucleation in IN 718,[9–13] IN 718DA,[40–42] and GH4169.[43,44] In particular, the observation of crack nucleation at carbide clusters (32 to 39 μm) in a fine-grained IN 718DA, which exhibits a mean grain size of 12 to 13 μm and a maximum grain size of 25 μm, appears to support the current model and the notion that the occurrence rates of individual anomalies need to be taken into account when considering competing crack nucleation mechanisms. Similarly, slip-induced facet formation was reported to occur at ALA grains on the order of 150 to 400 μm in the supersolvus microstructure of LSHR alloy with a mean grain size of 55 μm,[57,58] but the fatigue mechanism switched to inclusion-induced nucleation in the subsolvus microstructure with $\approx$5 μm mean grain size and 22 μm ALA grain size.[57,58] As the occurrence rates of

individual anomalies are reduced (*e.g.*, reducing the grain size, porosity, and inclusion size), previously unidentified or unknown crack nucleation mechanisms may emerge and become relevant. For examples, recent works have identified fatigue crack nucleation at twins or special boundaries in IN 718DA cyclically loaded in the very high cycle fatigue (VHCF) regime[40,41] and in Rene 88DT.[69]

V. CONCLUSIONS

A theoretical analysis has been performed to develop a scaling law for predicting the fatigue crack nucleation life of Ni-based superalloys with inclusions in their microstructures. The conclusions reached as the result of this investigation are as follows:

1. There exists a critical inclusion size below which fatigue nucleation life is not reduced by the presence of inclusions in the microstructure.
2. The fatigue life of inclusion-induced nucleation decreases with increasing inclusion size according to a power-law that relates the fatigue nucleation life to the inclusion size normalized by the critical inclusion size.
3. The critical inclusion size is a function of the shear moduli of the inclusion and the matrix, the slipband width impinging on the inclusion and the size of the matrix grains.
4. The presence of slipband facets and initiation-induced fatigue facets in LCF specimens tested under similar loading conditions is an indication of the existence of a critical inclusion size with the inclusion and grain sizes being at or near the transition point.
5. The transition from slip-induced nucleation and facet formation at large grains to inclusion-induced nucleation at small grain sizes is caused by a reduction of the enhanced matrix fatigue life with decreasing grain size by the presence of inclusions in the microstructure.
6. The proposed power-law scaling relation and the critical inclusion size are observed in several PM Ni-based alloys, as well as forged and AM Ni-based alloys.
7. The fatigue strength is predicted to scale with inclusion size to a power of − 1/2 when the fatigue limit (2Mk, where k is critical resolved shear stress for slip to occur) is small compared to the fatigue strength. The observed exponent may deviate from − 1/2 when 2Mk is not negligible.

ACKNOWLEDGMENTS

This work was supported by the US Air Force Metal Affordability Initiative (Agreement Order No. FA8650-14-2-5211A0#40) (Patrick Golden, Program Manager). The clerical assistance of Ms. Loretta Mesa and Ms. Adrianna Bosquez, both at SwRI, in the preparation of the manuscript is acknowledged. The views, opinions, and/or findings expressed are those of the author and should not be interpreted as representing the official views or policies of the Department of Defense or the U.S. Government.

APPENDIX

Using Eqs. [2], [5] andnd Eq. [7], it can be readily shown that Eq. [4] can be expressed as

$$N_i^I = \left[\frac{\zeta_S}{\left(\frac{2\sigma_a}{F_m} - 2Mk\right)}\right]^{1/\alpha}\left(\frac{\xi_o}{\xi}\right)^{-1/2}, \qquad [A1]$$

which can be rearranged to give

$$\left(\frac{\Delta S_{th}^I}{F_m} - 2Mk\right)\left[N_i^I\right]^{\alpha} = \zeta_S\left(\frac{\xi_o}{\xi}\right)^{-1/2}, \qquad [A2]$$

where $\Delta S_{th}^I = 2\sigma_a$ is the fatigue strength of the Ni-based alloy with inclusions. Similarly, Eq. [1] can be rearranged to give

$$\left(\frac{\Delta S_{th}^S}{F_m} - 2Mk\right)\left[N_i^S\right]^{\alpha} = \zeta_S, \qquad [A3]$$

where $\Delta S_{th}^S = 2\sigma_a$is the fatigue strength of the Ni-based superalloy without inclusions. Dividing Eq. [A2] by Eq. [A3] leads one to

$$\frac{\Delta S_{th}^I - 2F_m Mk}{\Delta S_{th}^S - 2F_m Mk} = \left(\frac{\xi}{\xi_o}\right)^{-1/2}, \qquad [A4]$$

which can be simplified to

$$\Delta S_{th}^I = \Delta S_{th}^S\left(\frac{\xi}{\xi_o}\right)^{-1/2} \qquad [A5]$$

when the 2Mk term is negligible compared to the fatigue strengths. When the 2Mk is not negligible, the threshold stress for inclusion-induced crack nucleation can be obtained from Eq. [A4] to give

$$\Delta S_{th}^I = 2F_m Mk + \left(\Delta S_{th}^S - 2F_m Mk\right)\left(\frac{\xi}{\xi_o}\right)^{-1/2}, \qquad [A6]$$

which shows the scaling of the threshold stress ΔS_{th}^I with the inclusion size is not exactly a power-law with the − 1/2 exponent when 2Mk is not zero, where k is the critical resolved shear stress for slip to occur.

REFERENCES

1. J. Lankford: *Int. Met. Rev.*, 1977, vol. 21, pp. 221–28.
2. J.C. Grosskreutz and G.G. Shaw: *Proceedings of 2nd International Conference on Fracture*, P.L. Pratt, E.H. Andrews, R.L. Bell, N.E. Frost, R.W. Nichols, and E. Smith, eds., Chapman and Hall, London, 1969, pp. 620–29.
3. C.Y. Kung and M.E. Fine: *Metall. Trans. A*, 1979, vol. 10A, pp. 603–10.

4. C.Q. Bowles and J. Schijve: *Int. J. of Fract.*, 1973, vol. 9, pp. 171–79.
5. R. Chang, W.L. Morris, and O. Buck: *Scripta Metall.*, 1979, vol. 13, pp. 191–94.
6. W.L. Morris and M.R. James: *Metall. Trans. A*, 1980, vol. 11A, pp. 850–51.
7. J.M. Hyzak and I.M. Bernstein: *Metall. Trans. A*, 1982, vol. 13A, pp. 33–43.
8. J.M. Hyzak and I.M. Bernstein: *Metall. Trans. A*, 1982, vol. 13A, pp. 45–52.
9. A. Pineau: in *High Temperature Materials for Power Engineering*, Part II, R. Bachelet, R. Brunetaud, D. Coutsouradis, P. Esslinger, J. Ewald, I. Kvernes, Y. Lindblom, D.B. Meadowcroft, V. Regis, R.B. Scarlin, K. Schneider, and R. Singer, eds., Kluwer Academic Press, Dordrecht, 1990, pp. 913–34.
10. F. Alexandre, S. Deyber, and A. Pineau: *Scripta Mater.*, 2004, vol. 50, pp. 25–30.
11. N. Späth, V. Zerrouki, P. Poubanne, and Y.J. Guedou: in *Superalloys 718, 625 and Various Derivatives*, E.A. Loria, ed., TMS (The Minerals, Metals & Materials Society), 2001, pp. 173–83.
12. Y. Ono, T. Yuri, H. Sumiyoshi, and E. Takeuchi: *Mater. Trans.*, 2004, vol. 45, No. 2, pp. 342–45.
13. P.R. Bhowal and A.M. Wusatowska-Sarnek: in *Superalloys 718, 625, 706 and Derivatives 2005*, E.A. Loria, ed., TMS, Warrdendale, PA, 2005, pp. 341–49.
14. C.E. Schamblen and D.R. Chang: *Metall. Trans. B*, 1985, vol. 16B, pp. 775–84.
15. D.R. Chang, D.D. Krueger, and R.A. Sprague: in *Superalloys 1984, Proceedings of the Fifth International Symposium on Superalloys*, M. Gell, C.S. Kortovich, R.H. Bricknell, W.B. Kent, and J.F. Radavich, eds., TMS (The Minerals, Metals & Materials Society), Warrendale, PA, 1984, pp. 245–73.
16. X. Xie, L. Zhang, M. Zhang, J. Dong, and K. Bain: in *Superalloys 2004*, K.A. Green, T.M. Pollock, H. Harada, T.E. Howson, R.C. Reed, J.J. Schirra, and S. Walston, eds., TMS (The Minerals, Metals & Materials Society), Warrendale, PA, 2004, pp. 451–58.
17. M.J. Caton, S.K. Jha, A.H. Rosenberger, and J.M. Larsen: in *Superalloys 2004*, K.A. Green, T.M. Pollock, H. Harada, T.E. Howson, R.C. Reed, J.J. Schirra, and S. Walston, eds., TMS (The Minerals, Metals & Materials Society), Warrendale, Pa, 2004, pp. 305–12.
18. W.J. Porter III, K. Li, M.J. Caton, S. Jha, B.B. Bartha, and J.M. Larsen: in *Superalloys 2008*, R.C. Reed, K.A. Green, P. Caron, T.P. Gabb, M.G. Fahrmann, E.S. Huron, and S.A. Woodard, eds., TMS (The Minerals, Metals & Materials Society), Warrendale, PA, 2008, pp. 541–48.
19. J. Gayda and R.V. Miner: *Int. J. Fatigue*, 1983, vol. 5 (3), pp. 135–43.
20. D.A. Jablonski: *Mater. Sci. Eng.*, 1981, vol. 48, pp. 189–98.
21. K. Zhao, X.-L. Liu, and Y.-H. He: *IOP Conference Series: Materials Science and Engineering 269*, IOP Publishing, 2017, p. 012005, https://doi.org/10.1088/1757-899x/269/1/012005.
22. T.P. Gabb, J. Telesman, P.T. Kantzos, and K. O'Connor: *Characterization of the Temperature Capabilities of Advanced Disk Alloy ME3*, NASA/TM-2002-211796, NASA Glenn Research Center, Cleveland, OH, 2002.
23. Honeywell Aerospace Inc.: DARPA Open Manufacturing Program Phase 3, Contract Number HR0011-12-C-0037, 2018.
24. K.S. Chan and A. Peralta-Duran: *Metall. Mater. Trans. A*, https://doi.org/10.1007/s11661-019-05309-7, published on-line, 21 June 2019.
25. G.T. Cashman: *Int. J. Fatigue*, 2010, vol. 32, pp. 492–96.
26. S.K. Jha, M.J. Caton, and J.M. Larsen: *Mat. Sci. Eng. A*, 2007, vols. 468–470, pp. 23–32.
27. K. Tanaka and T. Mura: *ASME J. Appl. Mech.*, 1981, vol. 48, pp. 97–102.
28. K. Tanaka and T. Mura: *Metall. Trans. A*, 1982, vol. 13A, pp. 117–23.
29. K.S. Chan: *Metall. Trans. A*, 2003, vol. 34A, pp. 43–58.
30. K.S. Chan: *Int. J. Fatigue*, 2010, vol. 32, pp. 1428–47.
31. A. de Bussac and J.C. Lautridou: *Fat. Fract. Eng. Mater. Struct.*, 1993, vol. 16, No. 8, pp. 861–84.
32. Y. Murakami and M. Endo: *Eng. Fract. Mech.*, 1983, vol. 17 (1), pp. 1–15.
33. Y. Murakami, S. Kodama, and S. Konuma: *Int. J. Fatigue*, 1989, vol. 11 (5), pp. 291–98.
34. J. Jiang, J. Yang, T. Zhang, F.P.E. Dunne, and T.B. Britton: *Acta Mater.*, 2015, vol. 97, pp. 367–79.
35. J. Jiang, J. Yang, T. Zhang, J. Zou, Y. Wang, F.P.E. Dunne, and T.B. Britton: *Acta Mater.*, 2016, vol. 117, pp. 333–44.
36. T. Zhang, J. Jiang, B. Britton, B. Shollock, and F. Dunne: *Proc. R. Soc. A.*, 2016, vol. 472, p. 20150792.
37. E.S. Huron and P.G. Roth: in *Superalloy 1996*, R.D. Kissinger, D.J. Deye, D.L. Anton, A.D. Cetel, M.V. Nathal, T.M. Pollock, and D.A. Woodford, eds., TMS (The Minerals, Metals & Materials Society), Warrendale, PA, 1996, pp. 359–67.
38. P. Kantzos, P. Bonacuse, J. Telesman, T. Gabb, R. Barrie, and A. Banik: in *Superalloy 2004*, K.A. Green, T.M. Pollock, H. Harada, T.E. Howson, R.C. Reed, J.J. Schirra, and S. Walston, eds., TMS (The Minerals, Metals & Materials Society), Warrendale, PA, 2004, pp. 409–17.
39. M.P. Enright and R.C. McClung: *Proceedings of ASME Turbo Expo 2010: Power for Land, Sea, and Air, GT2010-23618*, 14–18 June 2010, Glasgow, Scotland, UK.
40. D. Texier, J. Cormier, P. Villechaise, J.-C. Stinville, C.J. Torbet, S. Pierret, and T.M. Pollock: *Mater. Sci. Eng. A*, 2016, vol. 678, pp. 122–36.
41. D. Texier, A. Gómez, S. Pierret, J.-M. Franchet, T.M. Pollock, P. Villechaise, and J. Cormier: *Metall. Mater. Trans. A*, 2016, vol. 47A, pp. 1096–1109.
42. M. Abikchi, T. Billot, J. Crepin, A. Longuet, C. Mary, T.F. Morgeneyer, and A. Pineau: *Proceedings of 13th International Conference on Fracture*, 16–21 June 2013, Beijing, China.
43. X. Zhu, C. Gong, Y.-F. Jia, R. Wang, C. Zhang, Y. Fu, S.-T. Tu, and X-C. Zhang: *J. Mater. Sci. Technol.*, vol. 35, 2019, pp. 1607–17.
44. G.-J. Deng, S.-T. Tu, X.-C. Zhang, Q.-Q. Wang, and C.-H. Qin: *Eng. Fract. Mech.*, 2015, vol. 134, pp. 433–50.
45. A. Weidner, J. Man, W. Tirschler, P. Klapetek, C. Blochwitz, J. Polák, and W. Skrotzki: *Mater. Sci. Eng. A*, 2008, vol. 494, pp. 118–27.
46. A. Weidner, C. Blochwitz, W. Skrotzki, and W. Tirschler: *Mater. Sci. Eng. A*, 2008, vol. 479, pp. 181–90.
47. A. Weidner, R. Beyer, C. Blochwitz, C. Holste, A. Schwab, and W. Tirschler: *Mater. Sci. Eng., A*, 2006, vols. 435–436, pp. 540–46.
48. P. Lukáš and L. Kunz: *Mater. Sci. Eng. A*, 2001, vol. A314, pp. 75–80.
49. K. Obrtlík, P. Lukáš, and J. Polák: in *Low Cycle Fatigue and Elasto-Plastic Behaviour of Materials,* K.-T. Rie and P.D. Portella, eds., Elsevier, Amsterdam, 1998.
50. M. Risbet and X. Feaugas: *Eng. Fract. Mech.*, 2008, vol. 75, pp. 3511–19.
51. K.S. Chan, J.W. Tian, B. Yang, and P.K. Liaw: *Metall. Mater. Trans. A*, 2009, vol. 40A, pp. 2545–56.
52. A. Shyam and W.W. Milligan: *Acta Mater.*, 2004, vol. 52, pp. 1503–1513.
53. J.H. Zhang, Z.Q. Hu, Y.B. Xu, and Z.G. Wang: *Metall. Trans. A*, 1992, vol. 23A, pp. 1253–58.
54. J. Dahal, K. Maciejewski, and H. Ghonem: *Int. J. Fatigue*, 2013, vol. 57, pp. 93–102.
55. H.S. Ho, M. Risbet, and X. Feaugas: *Int. J. Fatigue*, 2017, vol. 102, pp. 1–8.
56. K.S. Chan: *Metall. Mater. Trans. A*, 2014, vol. 45A, pp. 3454–66.
57. T.P. Gabb, P.T. Kantzos, B. Palsa, J. Telesman, J. Gayda, and C.K. Sudbrack: in *12th International Symposium on Superalloys 2012*, E.S. Huron, R.C. Reed, M.C. Hardy, M.J. Mills, R.E. Montero, P.D. Portella, J. Telesman, eds., TMS (The Minerals, Metals & Materials Society), Warrendale, PA, 2012, pp. 63–72.
58. T.P. Gabb, P.T. Kantzos, J. Telesman, J. Gayda, C.K. Sudbrack, and B. Palsa: *Int. J. Fatigue*, 2011, vol. 33, pp. 414–26.
59. K.S. Chan: *Metall. Mater. Trans. A*, 2018, vol. 49A, pp. 5353–67.
60. W.E. Duckworth: *Metallurgia*, 1964, vol. 69, pp. 53–55.
61. R. Kiessling: *Non-Metallic Inclusions in Steels; Part 3: The Origin and Behavior of Inclusions and their Influence on the Properties of Steels*, The Iron and Steel Institute, London, UK, 1968.
62. N.E. Frost: *J. Mech. Phys. Solids*, 1961, vol. 9, pp. 143–51.
63. Z.G. Yang, G. Yao, G.Y. Li, S.X. Li, Z.M. Chu, W.J. Hui, H. Dong, and Y.Q. Weng: *Int. J. Fatigue*, 2004, vol. 26, pp. 959–66.

64. S.J. Hudak Jr., K.S. Chan, G.G. Chell, Y-D. Lee, and R.C. McClung: *Proceedings of David L. Davidson Symposium on Fatigue*, K.S. Chan, P.K. Liaw, R.S. Bellows, T.C. Zogas, and W.O. Soboyejo, eds., TMS, Warrendale, PA, 2002, pp. 107–20.
65. M.H. El Haddad, K.N. Smith, and T.H. Topper: *ASME J. Eng. Mater. Technol.*, 1979, vol. 101, pp. 42–46.
66. X.-F. Ma, Z. Duan, H.-J. Shi, R. Murai, and E. Yanagisawa: *J. Zhejiang Univ. Sci. A (Appl. Phys. Eng.)*, 2011, vol. 11, pp. 727–37.
67. Z.G. Yang, J.M. Zhang, S.X. Li, G.Y. Li, Q.Y. Wang, W.J. Hui, and Y.Q. Weng: *Mater. Sci. Eng. A*, 2006, vol. 427, pp. 167–74.
68. Q.Y. Wang, C. Bathias, N. Kawagoishi, and Q. Chen: *Int. J. Fatigue*, 2002, vol. 24, pp. 1269–74.
69. J. Miao, T.M. Pollock, and J.W. Jones: *Superalloys 2008*, by R.C. Reed, K.A. Green, P. Caron, T.P. Gabb, M.G. Fahrmann, E.S. Huron, and S.A. Woodard, eds., TMS (The Minerals, Metals & Materials Society), Warrendale, PA, 2008, pp. 589–97.